Superconductivity in compositionally complex cuprates with the $YBa_2Cu_3O_{7-x}$ structure

Aditya Raghavan,[1,*] Nathan D. Arndt,[1,*] Nayelie Morales-Colón,[1] Eli Wennen,[1] Megan Wolfe,[1] Carolina Oliveira Gandin,[1] Kade Nelson,[1] Robert Nowak,[2] Sam Dillon,[2] Keon Sahebkar,[1] and Ryan F. Need[1,†]

[1]*Department of Materials Science and Engineering, University of Florida, Gainesville, Florida 32611, USA*

[2]*Department of Physics, University of Florida, Gainesville, Florida 32611, USA*

(Received 21 September 2023; accepted 16 January 2024; published 20 February 2024)

High-temperature superconductivity is reported in a series of compositionally complex cuprates with varying degrees of size and spin point-defect disorder. Three compositions of Y-site alloyed $YBa_2Cu_3O_{7-x}$, i.e., (5Y)BCO, were prepared via solid-state methods using different sets of rare earth ions on the Y site. Synchrotron x-ray diffraction and energy-dispersive x-ray spectroscopy confirm these samples have high phase purity and homogeneous mixing of the Y-site elements. For samples near optimal doping, electrical resistivity and magnetometry measurements reveal the superconducting transition temperature, T_C, is greater than 91 K for all 5Y alloying compositions. The lack of T_C suppression observed in these materials, of order 1% relative to pure YBCO ($T_C = 93$ K), contrasts recent results on other multicomponent cuprates based on the La-214 system where superconductivity was not observed. Therefore, a key result from this work is the demonstration that high-temperature superconductivity can exist in complex ceramic compositions. The difference in superconducting behavior between these compositionally complex cuprate families is discussed in terms of impurity potentials and sample form (powder vs film). This work sets the stage for future studies to leverage the larger composition and disorder phase space of compositionally complex cuprates to isolate different types of disorder and their effect on the various electronic phases exhibited by high-T_C superconductors.

DOI: 10.1103/PhysRevMaterials.8.024801

I. INTRODUCTION

Disorder in superconductors has intrigued physicists and been the subject of numerous scientific studies over the past 60 years, starting with Anderson's theory and continuing to present day [1–6]. In *s*-wave superconductors, Anderson predicted that electron pairing survives nonmagnetic disorder in the weak disorder limit [1]. Later, Lee and Ma evaluated the strong disorder limit in *s*-wave systems and predicted increasing disorder would eventually cause a superconducting-insulator transition, as was subsequently observed in amorphous thin films [7,8]. By contrast, in unconventional *d*-wave superconductors, Abrikosov-Gor'kov (AG) theory predicts a universal T_C suppression even for weak nonmagnetic disorder, when that disorder is in or near the superconducting plane [9,10]. However, experimental evidence shows *d*-wave systems are more robust to disorder located away from the superconducting planes [11].

Recently, a new experimental approach to studying the the interplay of disorder and superconductivity has been enabled by the advent of high-entropy alloys (HEAs) [12]. HEAs are intermetallic compounds in which several elements (typically four or more) are alloyed together creating materials with large configurational entropy that thermodynamically favors the formation of single phase solid solutions with complex compositions. In 2014, the first superconducting HEA was reported in the compound $Ta_{34}Nb_{33}Hf_8Zr_{14}Ti_{11}$ with a transition temperature, T_C, of 7.3 K and type-II behavior [13]. Since then, many other superconducting HEAs have been successfully synthesized in a variety of different structure types [12,14,15]. To date, studies on HEA superconductors collectively demonstrate T_C values between those of amorphous alloys and simple binary alloys, which is consistent with the trend in *s*-wave systems that increasing disorder tends to suppress pairing and T_C [12].

More recently, this entropy-inspired materials engineering approach has been extended to cuprate *d*-wave systems [16,17]. These so-called high-entropy oxides (HEOs) are ionic analogs to HEAs, in which several elements are selectively substituted onto a specific ionic sublattice by judicious choice of ion size and valence [18]. Thus far, studies of HEO cuprates have only focused on the RE_2CuO_4 (RCO) system with the Ruddlesden-Popper structure and alloying on the rare earth (RE) site [16,17], hereafter denoted (5R)CO. Musicó *et al.* compared synthetic routes for bulk powders using only trivalent ions and showed both traditional solid-state and sol-gel methods were able to produce well-mixed, single-phase material; however, no attempt was made to charge dope that material into the superconducting phase [16]. The other two studies grew (5R)CO as epitaxial thin films using (5R)CO targets and pulsed laser deposition [17,19] and attempts were made to optimally charge dope both (5R)CO films using both hole and electron dopants. However, all samples showed insulating behavior regardless of doping. Using x-ray absorption measurements of the Cu coordination environment, Mazza *et al.* attributed this result to large distortion with the Cu-O

*These authors contributed equally to this work.
†Corresponding author: rneed@ufl.edu

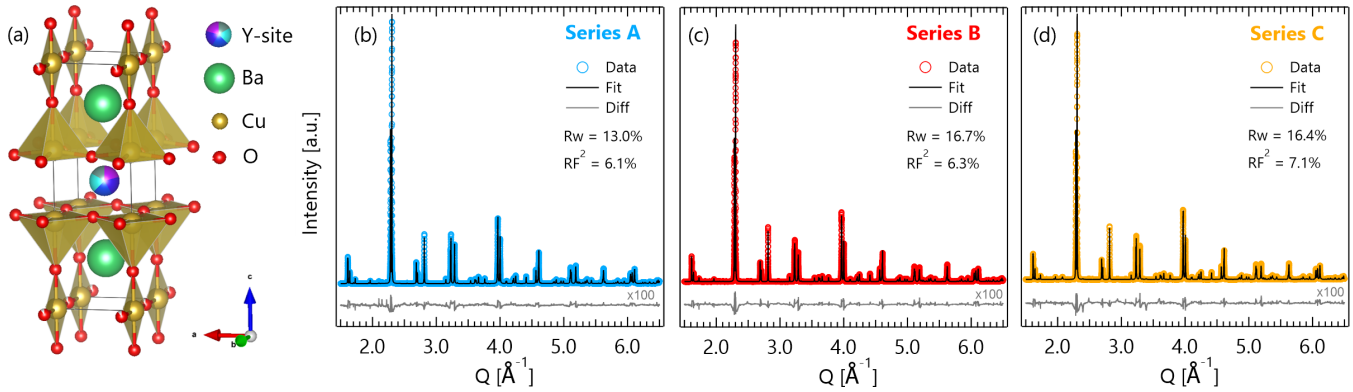

FIG. 1. (a) *Pmmm* crystal structure of (5Y)BCO with five elements alloyed on the Y site. (b)–(d) Reitveld refinements of synchrotron x-ray diffraction data (APS, 11-BM) for each of the three Y-site compositions. The difference curve is weighted by the standard uncertainty defined as $(Data - Fit)/\sqrt{Data}$ and scaled by 100× for visibility. The weighted residual, R_W, is a goodness-of-fit metric of the whole data set, while the unweighted phase residual, RF^2, is specific to the (5Y)BCO phase.

plane originating from size variance of the ions substituted onto the RE site [17].

Here, we report the synthesis and behavior of HEO cuprates that exhibit high-T_C superconductivity. Specifically, compositionally complex variants of $YBa_2Cu_3O_{7-x}$ were created by alloying three different sets of trivalent (isovalent) ions onto the Y site to create three, unique (5Y)BCO compositions with varying degrees of size and spin disorder, parametrized by the ion radii variance and average spin, respectively. High phase purity and elemental mixing for all three (5Y)BCO compositions was confirmed by synchrotron diffraction and electron microscopy. All compositions exhibited T_C values between 91 K and 92 K near optimal oxygen doping and ac magnetometry confirmed these transitions to be superconducting. The lack of observed T_C suppression in (5Y)BCO demonstrates that pairing in this structure type can be remarkably robust to disorder on the Y site. These results are discussed in terms of impurity potentials and their contrast with recent experiments on (5R)CO.

II. RESULTS

Powder batches of each (5Y)BCO composition were prepared by weighing out stoichiometric amounts of metal oxide and metal carbonate precursors followed by manual grinding, room-temperature pellet pressing, and firing in a muffle furnace at dwell temperatures ranging from 900 °C to 1000 °C. Each set of Y-site ions was selected to have an average ionic radius close that of yttrium to minimize lattice strain and long-range structural distortions. Only trivalent substitutional ions were used to prevent charge doping differences between series. Doping in these samples is instead due to oxygen vacancies, the concentration of which was controlled by the quench rate during synthesis with an optimal cooling rate of 1 °C/min for all series. Synthesis conditions were optimized using phase purity and transition temperature as the primary metrics. These metrics were evaluated respectively using laboratory x-ray diffraction (XRD) collected on a Panalytic MPD (Cu Kα) and four-point probe measurements taken with a Quantum Design Versalab. Dozens of samples of each composition were produced during the synthesis optimization. However, the results presented in the main text were collected from a total of five samples made using recipes confirmed to reproducibly generate samples that appear phase pure when characterized by these methods.

The room-temperature average crystal structure for each composition of (5Y)BCO was determined using high-resolution synchrotron XRD measurements collected at Argonne National Lab's Advanced Photon Source 11-BM beamline and refined using the Rietveld method implemented in GSAS-II. Figure 1 shows the synchrotron XRD data and fits corresponding to the orthorhombic *Pmmm* structure exhibited by pure YBCO and expected for our (5Y)BCO samples. The *Pmmm* phase fraction ranges from 99.5% in the series A sample to a minimum of 97.5% in the series C sample. The remaining peaks index to trace amounts of unreacted binary precursors and the intermediate ternary phase $BaCuO_2$. The difference curves show the largest remaining error in the fits corresponds to peak shape mismatch on the *Pmmm* peaks. This confirms the impurities are small enough and sufficiently well fit so as not to limit the refinement accuracy of the (5Y)BCO *Pmmm* phase.

The refined structural parameters for each (5Y)BCO composition are reported in Table I alongside a list of the substitutional Y-site elements, their average ionic radii, size disorder, and average number of unpaired spins. Size disorder (σ^2) is quantified as the variance of the ionic radii of the elements on the Y-site defined as $\sigma^2 = \sum_i x_i r_i^2 - r_A^2$, where $r_A = \sum_i x_i r_i$ is the average ionic radius of the A-site cation and x_i is the fraction of the ith cation of radius r_i. Several notable trends are seen in these refinement results. First, a larger unit cell (0.2–0.4%) is refined for each (5Y)BCO composition compared to pure YBCO. This unit cell expansion is primarily due to elongation of the c axis (0.1–0.2%) and much smaller expansions are mostly observed along the a and b axes. In the case of C series, the a axis appears to shorten slightly. Second, the (5Y)BCO unit cell volumes and c-axis lattice constants are directly correlated with the average ionic radius of the Y-site element mixture. This is consistent with a picture that isovalent Y-site alloying creates expansive chemical pressure along the c axis. However, unit cell and c-axis expansion still occur in C series, where the average

TABLE I. Structural information for the different compositions of (5Y)BCO. Ionic radii (I.R.) and variance are calculated using eightfold coordinate values from the Shannon-Prewitt tables [20]. Lattice parameters and bond angles are taken from Rietveld refinement of the synchrotron data. Error on all refined lattice parameters is smaller than the final decimal place by at least one order of magnitude. Values for unalloyed YBCO are taken from Ref. [21].

	Y-site (calculated)				*Pmmm* Parameters (refined)					
Series	Composition	Average I.R. (Å)	Variance I.R. (Å^2)	Unpaired Spins	a [Å]	b [Å]	c [Å]	V [Å^3]	Avg. Cu-O-Cu Angle [deg.]	Variance Cu-O-Cu Angle [deg.^{2}]
-	Y	1.0190	0	0	3.8210(2)	3.8826(3)	11.6720(8)	173.16	164.85	0.0025
A	$Y_{0.2}Ho_{0.2}Dy_{0.2}Gd_{0.2}Yb_{0.2}$	1.0198	0.00048	3.4	3.8232	3.8901	11.6973	173.97	163.49	0.3136
B	$Y_{0.2}Ho_{0.2}Dy_{0.2}Gd_{0.2}Lu_{0.2}$	1.0182	0.00060	3.2	3.8243	3.8892	11.6923	173.90	163.89	2.1756
C	$Y_{0.2}Ho_{0.2}Er_{0.2}Tb_{0.2}Yb_{0.2}$	1.0126	0.00033	2.8	3.8197	3.8863	11.6833	173.43	164.50	4.4100

Y-site ionic radius is significantly smaller than Y^{3+}, which one expects to cause *c*-axis compression from a simple chemical pressure model. This suggests a tensile strain contribution exists along the *c* axis in these disordered (5Y)BCO compounds, which is separate from and adds to the chemical pressure expected from having different average ionic radius on the Y site. However, in entropy-alloyed (5R)CO, *c*-axis contraction and smaller unit cells were observed upon adding disorder to the La site [16], which suggests that a pure chemical pressure model is insufficient to fully explain the effect of the disorder on structure in these materials.

The sXRD refinement results also indicate that Y-site alloying changes the Cu-O-Cu bond angles in the CuO_2 planes that carry supercurrent. On average, the Cu-O-Cu bond angles in the CuO_2 plane are smaller in (5Y)BCO than pure YBCO. However, the (5Y)BCO samples appear to have greater variance of the Cu-O-Cu bond angles (i.e., greater difference between Cu-O2-Cu vs Cu-O3-Cu angles) than pure YBCO. Interestingly, variance in the Cu-O-Cu bond angles correlates with decreasing average ionic radii on the Y site, rather than with the variance of the ionic radii.

In addition to the average atomic structures, the microscale chemical homogeneity and element clustering in these samples was established using element-specific composition maps collected with energy dispersive x-ray spectroscopy on sintered pellets in a FEI Nova 430 scanning electron microscope (SEM-EDS). Figure 2 shows a series of high magnification maps from a representative series C sample that was "phase pure" to laboratory XRD. Note that the scale bars for each panel are 2 μm; this is slightly larger than the smallest meaningful length scale in these images, which is defined by the electron beam's interaction volume from which the x rays are emitted, which is approximately 1 μm. The most notable contrast appears in the same location in each map, as dark regions in the upper left side and upper right corner. This is demonstratively from sample topography as shown in the inset of Fig. 2(a). Aside from the topographical contrast, each image and the combined overlay in panel (a) are homogeneous in color and intensity, indicating uniform mixing of all elements down to the smallest length scales accessible to our methods. Additional SEM-EDS maps are presented in Figs. S1– S5 for different compositions and magnifications [22]. Together, our SEM-EDS results show that samples that appear "phase pure" to laboratory-source XRD have very high elemental homogeneity at length scales 1 μm and above, which we define as having very few (0–1) visible elemental clusters or impurity phases larger than the 1 μm resolution.

Electrical resistivity measurements for such samples are shown in Fig. 3 for each (5Y)BCO composition series. Measurements were collected under 0 T and 3 T magnetic fields on pressed and sintered pellets and are plotted normalized to the resistivity value at 300 K. Note that all three samples presented here exhibit T-linear resistivity above T_C, which is known to occur primarily near optimal doping and the peak of the superconducting dome [23–26]. In lieu of directly measured oxygen concentrations, which could not be accurately extracted from our sXRD refinements [22], the linearity of the resistivity data above T_C was used to optimize cooling rate and hole doping in our samples.

In the near-optimally doped samples shown in Fig. 3, all (5Y)BCO compositions show a sharp drop to zero resistance above 90 K. T_C values for the three samples range from 91.5 K to 92.5 K, calculated as the inflection point of the normalized resistance change. Application of a 3 T magnetic field suppresses and broadens the resistivity transition. This behavior is expected and has been reported previously for the parent YBCO and is associated with a multicritical point where the superconducting transition goes from first order to second order [27]. The T_C values for samples *within* a series were observed to vary on the order of 1 K from sample to sample, despite nominally identical synthesis procedures [22]. Therefore, no conclusions should be drawn from the order of T_C values presented in Fig. 3 with respect to their chemical or structural differences, as T_C ordering is not repeatable. What is repeatable is that, for an optimized synthesis procedure, T_C was always observed to be >91 K, indicating that the spin and lattice disorder added to the system do not greatly disrupt the pairing interaction.

The superconducting nature of the resistivity transition was verified using ac susceptibility measurements, collected in a Quantum Design MPMS3 Superconducting Quantum Interference Device (SQUID) magnetometer. Figure 4 shows ac susceptibility data collected on the same series A sample shown in Fig. 3. χ' and χ'' are the real and imaginary parts of susceptibility of the material, respectively, and the divergence between the two marks the superconducting transition temperature T_C. For series A under zero-field cooling, this divergence occurs just above 92.5 K, which is in perfect agreement with

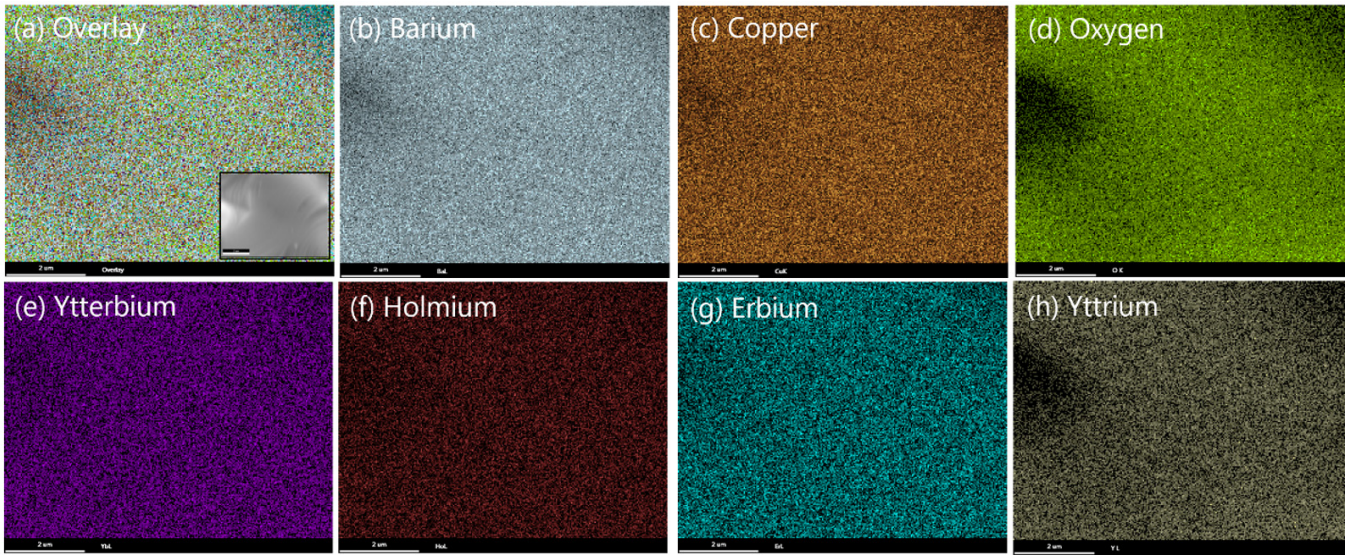

FIG. 2. High magnification composition maps taken with SEM-EDS on a series C sample. Individual panels show intensity proportional to the following x-ray edges: (a) an overlay of one edge mapped for each series C (5Y)BCO element, (b) Ba K, (c) Cu K, (d) O K, (e) Yb L, (f) Ho L, (g) Er L, and (h) Y L. The scale bar below each panel is 2 microns. Inset in (a) is a secondary electron image showing the uneven surface topography of the sintered pellet that gives rise to a shape-induced contrast artifact common to all these maps but more prevalent for lighter elements.

the start of the resistance downturn in Fig. 3. The peak in χ'' occurs near 92 K, which aligns with the inflection of the resistance transition in this sample. The downturn in χ' confirms the diamagnetic Meissner state below T_C. Additionally, the shape of the χ'' peak gives information about flux pinning in these samples. Under the zero field, the χ'' peak is narrow, suggesting strong, uniform flux pinning sites in the Meissner state. Under a 3 T applied field, the χ'' peak broadens and shifts lower in temperature, reflecting a weaker and wider range of pinning interactions in the type-II vortex state.

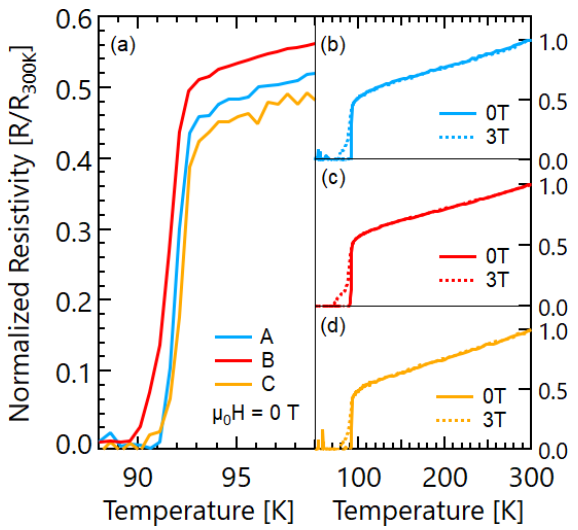

FIG. 3. Electrical resistivity measurements normalized to the resistivity at 300 K. (a) Zero-field-cooled (0 T) normalized resistivity shown near the superconducting transition. (b)–(d) Full temperature range showing T-linear behavior above T_C for series A, B, and C, respectively.

III. DISCUSSION

The key result from this study is the unambiguous observation of high-temperature superconductivity in a series of compositionally complex cuprates with disordered YBCO structures. This result and the (5Y)BCO compounds introduced here are intriguing for several reasons: (1) the lack of T_C suppression, (2) the contrasting superconducting behavior with doped (5R)CO films, and (3) the potential for these compositionally complex cuprates to help disentangle different types of disorder induced physics in high-temperature d-wave superconductors.

Considering first the minimal T_C suppression observed in (5Y)BCO, this result is in fact to be expected and consistent with prior theory and experiment on chemically simpler

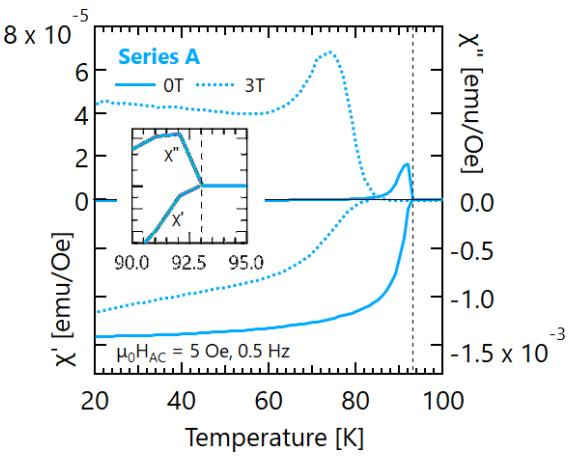

FIG. 4. Zero-field-cooled (0 T) and field-cooled (3 T) ac magnetic susceptibility measurements from a series A sample. Inset shows a closeup of the zero-field transition.

YBCO alloys. For example, several studies have alloyed a single element onto the Y site of YBCO and observed similarly minimal T_C suppression [28–31]. Theoretically, the concept of impurity potentials provides a framework for comparing the degree to which different impurities are expected to disrupt pairing and suppress superconductivity. The strength of impurity potentials in cuprates depends both on the distance of the impurity from the superconducting plane and its charge difference with the parent ion on the impurity site [32,33]. Because only isovalent impurities were used in this study, the (5Y)BCO lattice "sees" no apparent charge disorder and thus impurity potentials are generally expected to be weak in these compounds. This implies minimal pairing disruption should be expected here and agrees well with the near-maximum T_C values we observed.

Impurity potentials also provide one way to understand the contrasting appearance of superconductivity seen between the two compositionally complex cuprate families reported thus far: (5Y)BCO and (5R)CO. In both systems, the disordered site is plaquette centered above the CuO_2 square lattice and roughly the same distance from the CuO_2 plane. Specifically, in YBCO, the Y site sits roughly 3.2 Å from Cu and 2.4 Å from O, while in the T′-(5R)CO structure, the RE site sits slightly further away at 3.2–3.3 Å from Cu and 2.7 Å from O [21,34]. These small differences between the Y-site and La-site position with respect to its neighboring CuO_2 plane suggest these materials should experience similar impurity potentials for *isovalent* disorder on these sites. However, charge doping (5R)CO requires use of divalent or tetravalent ions on the RE site, which creates a charge difference on the RE site relative to trivalent La and therefore significantly increases the impurity potential in the (5R)CO system. Thus larger impurity potentials are expected for the doped (5R)CO than (5Y)BCO with oxygen doping, which could explain the lack of superconductivity observed in those samples.

Alternatively, Mazza *et al.* proposed that the large cation-size disorder on the RE site was the reason their (5R)CO samples did not superconduct [17]. Using the Shannon-Prewitt ionic radii [20], the reported (5R)CO samples have calculated size disorder parameters of 0.0025 and 0.0030 $Å^2$ for the electron- and hole-doped samples, respectively. By comparison, the (5Y)BCO samples reported here have size disorder parameters that vary from 0.0003 to 0.0006 $Å^2$, approximately one order of magnitude smaller than the (5R)CO samples. This analysis is consistent with the authors' hypothesis that large size disorder suppresses superconductivity in their (5R)CO samples. However, additional studies are required to determine whether differences in size disorder, impurity potential, or some combination is responsible for suppressing superconductivity in (5R)CO samples to date.

The open questions noted above regarding (5R)CO and (5Y)BCO highlight the broader future potential of compositionally complex cuprates: to isolate different types of disorder from one another structurally and thereby allow disorder-dependent properties, like superconductivity, magnetism, and non-Fermi liquid conduction to be controlled and studied in new ways. This broader potential rests on two key ways in which disorder can arguably be controlled better in compositionally complex oxides than simple oxide alloys. First, by carefully picking the substitutional element series, the degree of spin and lattice character in the *atomic-scale, point-defect* disorder can be decoupled. For example, consider substituting Gd^{+3} (IR = 1.053 Å, S = for Y^{+3}; IR = 1.019 Å, S = 0) in YBCO, where changes in the average Y-site ionic radius (lattice distortion) cannot be separated from changes in the average Y-site moment (spin distortion). The (5Y)BCO compositions studied here demonstrate, weakly, this ability to decouple the spin and lattice degrees of freedom. However, a simple consideration of the available trivalent ions on the Periodic Table proves a wider spin-lattice distortion phase space (combinations) is possible using an entropy-enhanced multicomponent alloying approach. In addition to the larger composition and disorder phase space, "high-entropy" materials often exhibit properties that deviate from the traditional mixing rules observed in single-component alloys. This phenomenon has already been observed in the dielectric and magnetic behavior of HEOs [35–38] and is likely to manifest in interesting ways in the already complex high-T_C phase diagram.

In addition, there is a growing idea within HEA and HEO literature that the extent (i.e., volume fraction) and length scale of *microstructural* disorder, like chemical clustering and phase precipitation, can be controlled by the kinetics of synthesis [39,40]. Previous literature and our own SEM-EDS results prove that it is possible to create HEO microstructures with varying degrees of chemical clustering. The open challenges are to explain why and how that process occurs in different HEOs and then control it. With design control over *both atomic- and microstructure disorder* in HEOs, many more questions and experiments open up regarding the use of disorder to control functional oxide properties. For example, in the case of cuprate superconductors, a recently proposed theory predicts that the length scale of disorder, whether pointlike or extended, will have different effects on the strange metal phase behavior [41]. This could be tested using a series of (5Y)BCO samples where disorder is controlled across multiple length scales. Similar approaches could be used to shed light on the behavior of other complex oxide families, like relaxor ferroelectrics or frustrated magnets, where both pointlike and extended defects are known to impact material properties [42,43].

In conclusion, this work reports high-temperature superconductivity in a family of compositionally complex cuprate superconductors. Three compositions of (5Y)BCO were made with high phase purity and T_C values greater than 91 K. The negligible T_C reduction relative to undisordered YBCO is consistent with prior work on simpler YBCO alloys and a theoretical framework of weak impurity potentials in isovalently alloyed systems. The contrasting behavior of (5Y)BCO with recent reports of compositionally complex (5R)CO highlights the sensitive nature of d-wave superconductivity to different types of disorder and provides opportunities for future studies.

ACKNOWLEDGMENTS

We thank T. Z. Ward, P. J. Hirschfeld, and M. M. Butala for helpful conversations framing the project and interpreting the results. This work was supported by UF Research. N.M.-C. and E.W. were supported by the NSF REU program (Grant No. DMR-2244024).

A.R., N.D.A., and R.F.N. conceptualized the project and designed the experiments. Samples were synthesized and characterized by A.R., N.M.-C., S.D., R.N., E.W., M.W., C.O.G., and K.N. Synchrotron measurements were prepared by A.R. and K.S. and analyzed by A.R. and R.F.N. N.D.A. collected the magnetometry. A.R. and R.F.N. wrote the first manuscript draft. All authors contributed to the final version.

[1] P. W. Anderson, J. Phys. Chem. Solids **11**, 26 (1959).

[2] M. P. A. Fisher, Phys. Rev. Lett. **65**, 923 (1990).

[3] S. H. Pan, J. P. O'Neal, R. L. Badzey, C. Chamon, H. Ding, J. R. Engelbrecht, Z. Wang, H. Eisaki, S. Uchida, and A. K. Gupta, Nature (London) **413**, 282 (2001).

[4] Y. Dubi, Y. Meir, and Y. Avishai, Nature (London) **449**, 876 (2007).

[5] B. Sacépé, T. Dubouchet, C. Chapelier, M. Sanquer, M. Ovadia, D. Shahar, M. Feigel'man, and L. Ioffe, Nat. Phys. **7**, 239 (2011).

[6] Y. Mizuguchi, H. Usui, R. Kurita, K. Takae, M. R. Kasem, R. Matsumoto, K. Yamane, Y. Takano, Y. Nakahira, A. Yamashita, Y. Goto, A. Miura, and C. Moriyoshi, Mater. Today Phys. **32**, 101019 (2023).

[7] M. Ma and P. A. Lee, Phys. Rev. B **32**, 5658 (1985).

[8] A. F. Hebard and M. A. Paalanen, Phys. Rev. Lett. **65**, 927 (1990).

[9] A. A. Abrikosov and L. P. Gor'kov, Zh. Eksp. Teor. Fiz. **39**, 1782 (1960).

[10] S. K. Tolpygo, J.-Y. Lin, M. Gurvitch, S. Y. Hou, and J. M. Phillips, Phys. Rev. B **53**, 12454 (1996).

[11] K. Fujita, T. Noda, K. M. Kojima, H. Eisaki, and S. Uchida, Phys. Rev. Lett. **95**, 097006 (2005).

[12] L. Sun and R. J. Cava, Phys. Rev. Mater. **3**, 090301 (2019).

[13] P. Koželj, S. Vrtnik, A. Jelen, S. Jazbec, Z. Jagličić, S. Maiti, M. Feuerbacher, W. Steurer, and J. Dolinšek, Phys. Rev. Lett. **113**, 107001 (2014).

[14] F. Von Rohr, M. J. Winiarski, J. Tao, T. Klimczuk, and R. J. Cava, Proc. Natl. Acad. Sci. USA **113**, E7144 (2016), .

[15] D. Hirai, N. Uematsu, K. Saitoh, N. Katayama, and K. Takenaka, Inorg. Chem. **62**, 14207 (2023).

[16] B. L. Musicó, Q. Wright, C. Delzer, T. Z. Ward, C. J. Rawn, D. G. Mandrus, and V. Keppens, J. Am. Ceram. Soc. **104**, 3750 (2021).

[17] A. R. Mazza, X. Gao, D. J. Rossi, B. L. Musico, T. W. Valentine, Z. Kennedy, J. Zhang, J. Lapano, V. Keppens, R. G. Moore, M. Brahlek, C. M. Rost, and T. Z. Ward, J. Vac. Sci. Technol. A **40**, 013404 (2022).

[18] C. M. Rost, E. Sachet, T. Borman, A. Moballegh, E. C. Dickey, D. Hou, J. L. Jones, S. Curtarolo, and J.-P. Maria, Nat. Commun. **6**, 8485 (2015).

[19] W. Zhang, A. R. Mazza, E. Skoropata, D. Mukherjee, B. Musico, J. Zhang, V. M. Keppens, L. Zhang, K. Kisslinger, E. Stavitski, M. Brahlek, J. W. Freeland, P. Lu, and T. Z. Ward, ACS Nano **14**, 13030 (2020).

[20] R. D. Shannon, Acta Crystallogr., A **32**, 751 (1976).

[21] Y. Z. Nozik, E. Kuklina, G. Schuster, L. Weiss, and V. Matts, Sov. Phys. Crystallogr. **36**, 125 (1991).

[22] See Supplemental Material at http://link.aps.org/supplemental/10.1103/PhysRevMaterials.8.024801 for additional details regarding the sXRD refinement methodology and results, EDS micrographs showing sample homogeneity and Y-site element mixing, and a comparison of transport behavior and variability within a sample series.

[23] M. Gurvitch and A. T. Fiory, Phys. Rev. Lett. **59**, 1337 (1987).

[24] B. Keimer, S. A. Kivelson, M. R. Norman, S. Uchida, and J. Zaanen, Nature (London) **518**, 179 (2015).

[25] M. Le Tacon, Science **373**, 1438 (2021).

[26] P. W. Phillips, N. E. Hussey, and P. Abbamonte, Science **377**, eabh4273 (2022).

[27] R. M. Langan, S. N. Gordeev, P. A. J. de Groot, A. G. M. Jansen, R. Gagnon, and L. Taillefer, Phys. Rev. B **58**, 14548 (1998).

[28] A. R. Devi, V. S. Bai, P. V. Patanjali, R. Pinto, N. H. Kumar, and S. K. Malik, Supercond. Sci. Technol. **13**, 935 (2000).

[29] J. L. MacManus-Driscoll, S. R. Foltyn, B. Maiorov, Q. X. Jia, H. Wang, A. Serquis, L. Civale, Y. Lin, M. E. Hawley, M. P. Maley, and D. E. Peterson, Appl. Phys. Lett. **86**, 032505 (2005).

[30] T. J. Haugan, T. A. Campbell, N. A. Pierce, M. F. Locke, I. Maartense, and P. N. Barnes, Supercond. Sci. Technol. **21**, 025014 (2008).

[31] S. H. Wee, E. D. Specht, C. Cantoni, Y. L. Zuev, V. Maroni, W. Wong-Ng, G. Liu, T. J. Haugan, and A. Goyal, Phys. Rev. B **83**, 224520 (2011).

[32] S. Graser, P. J. Hirschfeld, L.-Y. Zhu, and T. Dahm, Phys. Rev. B **76**, 054516 (2007).

[33] H. U. Özdemir, V. Mishra, N. R. Lee-Hone, X. Kong, T. Berlijn, D. M. Broun, and P. J. Hirschfeld, Phys. Rev. B **106**, 184510 (2022).

[34] M. Tuilier, B. Chevalier, A. Tressaud, C. Brisson, J. Soubeyroux, and J. Etourneau, Physica C **200**, 113 (1992).

[35] C. Oses, C. Toher, and S. Curtarolo, Nat. Rev. Mater. **5**, 295 (2020).

[36] D. Bérardan, S. Franger, D. Dragoe, A. K. Meena, and N. Dragoe, Phys. Status Solidi RRL **10**, 328 (2016).

[37] P. B. Meisenheimer, T. J. Kratofil, and J. T. Heron, Sci. Rep. **7**, 13344 (2017).

[38] A. R. Mazza, E. Skoropata, Y. Sharma, J. Lapano, T. W. Heitmann, B. L. Musico, V. Keppens, Z. Gai, J. W. Freeland, T. R. Charlton, M. Brahlek, A. Moreo, E. Dagotto, and T. Z. Ward, Adv. Sci. **9**, 2200391 (2022).

[39] Z. An, S. Mao, T. Yang, C. T. Liu, B. Zhang, E. Ma, H. Zhou, Z. Zhang, L. Wang, and X. Han, Mater. Horiz. **8**, 948 (2021).

[40] G. N. Kotsonis, S. S. Almishal, F. Marques dos Santos Vieira, V. H. Crespi, I. Dabo, C. M. Rost, and J.-P. Maria, J. Am. Ceram. Soc. **106**, 5587 (2023).

[41] A. A. Patel, H. Guo, I. Esterlis, and S. Sachdev, Science **381**, 790 (2023).

[42] A. A. Bokov and Z.-G. Ye, J. Mater. Sci. **41**, 31 (2006).

[43] O. A. Starykh, Rep. Prog. Phys. **78**, 052502 (2015).